Balogun and Fayemi
Journal of Analytical Science and Technology (2023) 14:30
https://doi.org/10.1186/s40543-023-00396-z

Journal of Analytical Science and Technology

RESEARCH ARTICLE

Open Access

Impedance and voltammetry detection of bromate in food samples using NiPcMWCNTs modified glassy carbon electrode

Sheriff Aweda Balogun[1,2] and Omolola Esther Fayemi[1,2*]

Abstract

A sensitive bromate sensor was developed using nickel phthalocyanine multi-walled carbon nanotubes nanocomposite modified on a glassy carbon electrode. The NiPcMWCNTs nanocomposite was prepared from nickel nanoparticles, phthalocyanine, and functionalized MWCNTs via ultrasonication. UV–visible spectroscopy, SEM, XRD, TEM, and EDX techniques were used to verify the successful fabrication of the nanomaterials. The results of the EIS and CV experiments conducted in 5 mM $K_3(Fe(CN)_6/K_4(Fe(CN)_6$ made in 0.1 M of PBS (pH 7) revealed that the NiPcMWCNTs/GCE exhibited higher current response, faster electron transfer, and high specific capacitance compared to other electrodes. The electrochemical reduction of bromate was actualized in 0.1 M H_2SO_4 (pH 1) using EIS and SWV techniques. Using the EIS technique, an LoD of 6.72 μM was obtained with a sensitivity of 483.7 μA μM^{-1} over a linear dynamic range (LDR) of 24–100 μM. Whereas, with the SWV technique, a lower LoD (1.47 μM) was obtained with a higher sensitivity (1293 μA μM^{-1}) over an LDR of 12–56 μM. The developed sensor was characterized by good selectivity, high stability (95.5%), and good reproducibility (% RSD; 3.5%). The fabricated sensor was effectively used to detect bromate in bread samples with a good recovery rate, demonstrating the practical application of the sensor to detect bromate in real samples (bread).

Keywords Bromate, Nickel phthalocyanine, Multi-walled carbon nanotubes, Electrochemical sensors, Electrochemical impedance spectroscopy

Introduction

Despite bromate's usefulness in water treatment and food production, there are several instances of its negative impact on human health. Peripheral neuropathy, renal problems, and anemia have all been specifically linked to bromate intake (Crofton 2006; Fawell and Walker 2006) if ingested beyond the World Health Organization's authorized threshold of 25 μg L^{-1} (WHO 1996). It has also been linked to malignant growth in laboratory animals. Additionally, increased incidences of kidney tumors, thyroid cells, and peritoneal mesotheliomas have been associated with bromate in mice's and rats' drinking water. Human and animal auditory functions are also affected due to high bromate intake, according to scientific evidence (Balamurugan and Chen 2007). The World Health Organization, together with the US Environmental Protection Agency (USEPA), has set 0.078 μM (10 μg L^{-1}) as the maximum acceptable level (MAL) owing to its carcinogenicity (Organization and WHO 2004). Bromate in food and water has been linked to cancer risks for lifetime exposures, and the toxicological investigations by WHO (1996) have categorized bromate as a group B2 carcinogen in foods and water (Shanmugavel et al. 2020).

*Correspondence:
Omolola Esther Fayemi
Omolola.Fayemi@nwu.ac.za
[1] Department of Chemistry, Faculty of Natural and Agricultural Sciences, North-West University (Mafikeng Campus), Private Bag X2046, Mmabatho 2735, South Africa
[2] Material Science Innovation and Modelling (MaSIM) Research Focus Area, Faculty of Natural and Agricultural Sciences, North-West University (Mafikeng Campus), Private Bag X2046, Mmabatho 2735, South Africa

Also, the present techniques for its detection have significant limitations that necessitate the development of new and more efficient techniques for detecting BrO_3^- at trace levels, entailing fast, economic, reliable, highly selective, and sensitive analytical techniques.

Ion chromatography, gas chromatography, and spectrophotometry liquid chromatography (Kim and Shin 2012; Rahali et al. 2011; Snyder et al. 2005; Zakaria et al. 2011) are previously employed techniques to detect bromate. However, tedious and time-demanding, special sample preparation, multiple extractions and hydrolysis, low sensitivity, high temperature requirements, costly and sophisticated instrumentation limit the usage of these techniques for bromate detection (Menendez-Miranda et al. 2013). Most of these setbacks can be addressed to a greater extent by employing electrochemical methods, which are recently being utilized because of their quick analysis period, no sample pre-treatment, accessibility, and environmental friendliness. Besides these, they offer high selectivity, high sensitivity, and a lower detection limit (Balogun and Fayemi 2022).

In recent times, metal nanoparticles have been extensively utilized in magnetic storage, sensors, ferrofluids, and imaging applications owing to their electronic, thermal, magnetic, catalytic, and optical properties compared to bulk metals (Goyal 2017). Remarkably, the magnetic nanoparticles of nickel, iron, and cobalt have received greater attention in the past decade as a result of their remarkable magnetic properties, such as high Curie temperatures, colossal magnetoresistance, low saturation magnetization, and a very large coercivity as well as their potential uses in numerous fields, such as sensors, catalysis, and memory storage devices (Balogun and Fayemi 2022; Eluri and Paul 2012). Nickel nanoparticles (NiNPs) stand out among these nanoparticles due to their potential applications in various fields and extraordinary properties (Ali et al. 2019). Nickel nanoparticles have demonstrated good electrocatalytic activity towards dopamine, ascorbic acid, uric acid (He et al. 2016), nitrite, glucose (Arikan et al. 2022; Kumar et al. 2020), ethanol, methanol, oxygen (Luo et al. 2022; Roodbari et al. 2022), catechol, and hydroquinone (Hassine et al. 2021).

Carbon nanotubes (CNTs) belong to the family of fullerene, which is composed of sp^2 hybridized carbon and forms a tube-like structure of graphene units. The use of CNTs as a sensor fabricating material has been strongly influenced by their electronic conductivity, specifically the rolled-up concentric graphene units of the multi-walled carbon nanotubes (MWCNTs). Scientists have come to appreciate MWCNTs as electrode modifiers in electrochemical sensor fabrication owing to their electronic conductivity, huge surface area, and chemical inertness (Oliveira and Morais 2018). Furthermore, it has been found that MWCNTs contribute to the enhancement of the stability and dispersion of metal oxide nanoparticles in a composite, including both metal oxide nanoparticles and MWCNTs (Puangjan et al. 2017). The improved chemical properties and the intrinsic electronic conductivity of MWCNTs favour their usage as a modifier for BrO_3^- sensor (Roodbari et al. 2022; Vilian et al. 2016; Zhou et al. 2012). This might be attributed to electrostatic interaction as well as potential π–π interaction between BrO_3^- and MWCNTs. Multi-walled carbon nanotubes are now used as electrochemical sensing materials to facilitate electron transfer reactions. This is because they have a large surface area, are strong mechanically, have great electrical conductivity, and are chemically stable (Balogun and Fayemi 2022).

A phthalocyanine (Pc) is a macrocyclic compound with a central planar molecule and a delocalized 18-π electron system on carbon–nitrogen double bonds (Balogun and Fayemi 2022). Phthalocyanine is one of the important chemicals with numerous applications, including electrochemical sensors, photovoltaic cells, electrocatalysis, liquid crystal materials, photodynamic therapy, catalysts, and photosensitizers, because of its good spectral performance and high stability (Das et al. 2012; Kaya et al. 2014; Wang et al. 2021). The presence of hydrogen bonds, coordination interactions, and van der Waal forces allows Pc to bind a variety of analytes in an indifferent way (Reddy 2020). In addition, the ability to accommodate about 70 different metal atoms within the rings and to vary the side chain substituents results in exceptional and efficient nanomaterials with different selectivity, stability, and sensitivity (Balogun and Fayemi 2022). Recently, the metal phthalocyanines (MPc) have garnered much attention due to their excellent catalytic properties. In metal phthalocyanine, the central metal ions play a significant role in its high catalytic activity (Qiu et al. 2022; Yadav et al. 2016). Besides, the exceptional electrocatalytic activity of nickel phthalocyanines (NiPc) for a variety of compounds, its quick electron transfer capability, and its rich redox chemistry have made it more widely used in sensor development (Shao et al. 2022). Additionally, the core metal of the NiPc can easily alter its coordination environment, thus significantly boosting its selectivity and catalytic activity. The ease with which organic groups can be substituted in the complex's axial and equatorial regions, resulting in a variety of functions for anchoring complexes in solid substrates, is one of NiPc's outstanding properties that makes it a superior material in fabricating electrochemical sensors (Han et al. 2017; Jiang et al. 2019; Li et al. 2022; Mei et al. 2022).

Phthalocyanines have been extensively researched for functionalizing CNTs since they exhibit diverse electrical and photoelectronic properties that increase the

efficiency of CNTs-based devices. Recent studies revealed that MPc-CNTs composites show improved current responses than individual MPc or CNTs (Mphuthi et al. 2017). Studies have shown that impregnating MPc composites with other highly conductive materials on working electrodes reduces redox overpotentials and improves electrode faradaic currents (Kantize et al. 2019; Winiarski et al. 2020). Notably, the conductivity of the metal phthalocyanine-based films is enhanced with the addition of metallic nanoparticles as well as carbon-based materials (MWCNTs, quantum dots, graphene, and SWCNTs) (Guaraldo et al. 2019). An electron transport improvement is achieved between the electrode's surface and the analytes adsorbed on the thin film by adding these conductivity-enhancing materials (Kantize et al. 2019).

Nickel phthalocyanine multi-walled carbon nanotubes (NiPcMWCNTs) nanocomposites are now used to make electrochemical sensors that can detect a wide range of analytes with high selectivity, a low limit of detection, a large current response, high sensitivity, great reproducibility and repeatability, a large capacitance, and excellent stability over a wide concentration range. Thus, this is the primary motive behind the widespread usage of these nanocomposites in constructing sensors with other conducting nanomaterials. The study, therefore, explored the advantages of the phthalocyanine and MWCNTs sizable surface area, as well as the MWCNTs and nickel nanoparticles' high electrical conductivity to fabricate a fast, low-cost, sensitive, and selective electrochemical sensor for bromate detection. As far as we know, no research has ever been done on using the glassy carbon electrode (GCE) modified with NiPcMWCNTs for bromate detection.

Materials, reagents, and instruments

Potassium bromate ($KBrO_3$), multi-walled carbon nanotubes (98%), ethylene glycol, 29H, 31H$^-$ phthalocyanine (Pc), potassium hexacyanoferrate IV ($K_4(Fe(CN)_6)$, *N,N*-dimethyl formamide (DMF), potassium hexacyanoferrate III ($K_3(Fe(CN)_6)$, sodium dihydrogen phosphate (NaH_2PO_4), and disodium hydrogen phosphate (Na_2HPO_4) were supplied by Sigma-Aldrich (Darmstadt, Germany). Sulfuric acid, hydrochloric acid (HCl), nickel chloride, hydrazine hydrate, sodium hydroxide (NaOH), and methanol were products of Glassworld Chemicals (Johannesburg, South Africa). All reagents were of analytical quality.

The nanoparticles and nanocomposites were characterized morphologically and structurally using various techniques. Transmission electron microscopy (TEM) was performed using a JEOL2100 instrument equipped with a LaB 6 electron gun from JEOL Ltd (Tokyo, Japan). X-ray diffraction spectrophotometry (XRD) was conducted using equipment from Bruker Company (Karlsruhe, Germany). Scanning electron microscopy (SEM) was carried out using a JEOL JSM-6610 LV instrument from Dearborn, Peabody, MA, USA. UV–visible spectrophotometry was performed using an Agilent Technology, Cary 300 series UV–Vis spectrometer from Darmstadt, Germany. Energy diffraction X-ray (EDX) was conducted using a JEOL JSM-6610 LV instrument from Dearborn, Peabody, MA, USA. Electrochemical and impedance spectroscopy (EIS) analyses were performed utilizing an Autolab Potentiostat PGSTAT 302 (Eco Chemie, Utrecht, The Netherlands), managed by GPES (version 4.9) software (Utrecht, The Netherlands). Simultaneously, the electrochemical impedance spectroscopy (EIS) measurements were acquired utilizing the Metrohm Autolab (FRA 32) NOVA 2.1.3 software (Utrecht, The Netherlands) with a frequency span of 100 kHz–0.1 Hz. The experiments were conducted using distilled water.

Nickel nanoparticles synthesis

Nickel nanoparticles (NiNPs) synthesis was achieved by adding 8 mL of 1 M NaOH to a solution of 800 mL of ethylene glycol containing a mixture of 2 g of nickel chloride and 10 mL of hydrazine hydrate. The reaction mixture was continuously stirred at 70 °C for 45 min in a closed bottle. The resultant black particles were washed thoroughly with absolute ethyl alcohol and kept under vacuum at 27 °C for 24 h (Wu et al. 2012).

Functionalization of raw MWCNTs

The raw MWCNTs underwent a treatment process to introduce –COOH functional groups onto their surface. The functionalization process entails introducing 100 mg of pristine multi-walled carbon nanotubes (MWCNTs) into a solution comprising 150 mL of concentrated sulfuric acid (H_2SO_4) and 50 mL of concentrated nitric acid (HNO_3). The concoction underwent thermal treatment for 5 h at 65 °C and an additional 8 h at 80 °C. The resulting mixture was subjected to multiple washes with distilled water until its pH was neutralized. The obtained black particles were kept in an oven at a temperature of 70 °C for 12 h (Lee et al. 2017).

NiPcMWCNTs nanocomposites preparation

The preparation of the nanocomposites entails solubilizing 3 mg of phthalocyanine Pc and 3 mg of NiNPs in 1 mL of DMF followed by sonication for 2 h. After adding 3 mg of fMWCNTs, the resultant mixture underwent sonication for an additional 2 h. By means of ultrasonication-assisted spontaneous adsorption, the fMWCNTs' surface was coated with nickel phthalocyanine nanoparticles (NiPc) (Balogun and Fayemi 2022).

Modification of GCE with nanocatalysts

Before the bare GCE was modified with the synthesized nanoparticles and the nanocomposite, preliminary electrode treatment was carried out. The bare GCE was initially cleaned on a Sic Emery paper containing aluminum oxide slurry. The bare GCE in this state was immediately washed with a copious amount of water to remove traces of aluminum oxide particles. To ensure complete cleaning, the bare GCE was subjected to ultrasonication inside a beaker containing distilled water for about 5 min, and afterward in methanol for another 5 min.

Using the drop-dry approach, the cleaned, unmodified GCE was treated with each of the nanocatalyst pastes. About 5 µL of the prepared paste of NiNPs, fMWCNTs, Pc, and NiPcMWCNTs were dropped on the cleaned GCE and dried in an oven for about 5 min at 50 °C. The resultant modified electrodes were labelled NiPcMWCNTs/GCE, fMWCNTs/GCE, Pc/GCE, and Ni/GCE.

Results and discussion

Energy dispersive X-ray (EDX)

The EDX spectra of nickel nanoparticles and NiPcMWCNTs nanocomposites, as shown in Fig. 1, reflect their elemental composition. The presence of oxygen and carbon in Fig. 1a (NiNPs spectrum) indicates intruded impurities from the precursors. Similarly, the chlorine and sulphur in Fig. 1b were from the reagents (concentrated HCl and H_2SO_4) used for functionalizing the rMWCNTs. The existence of nitrogen and carbon (signifying phthalocyanine), carbon and oxygen (signifying *f*MWCNTs), and nickel in Fig. 1b suggests that the NiPcMWCNTs nanocomposite was successfully fabricated.

X-ray diffraction (XRD)

The crystalline structures of the synthesized NiNPs, raw MWCNTs, fMWCNTs, and NiPcMWCNTs nanocomposite were determined using XRD. Figure 2a depicts the XRD diffractogram of NiNPs with three major diffraction peaks at 2θ = 44.5° (1 1 1), 51.9° (2 0 0), 76.5° (2 2 0) corresponding to face-centered cubic (FCC) of pure nickel nanoparticles. These diffraction peaks appear similar to the ones reported for NiNPs in literature (Eluri and Paul 2012; Wu et al. 2012; Wu et al. 2010), affirming the successful synthesis of FCC pure nickel nanoparticles. Using Scherrer's equation (Klug and Alexander 1974), 12 nm was obtained as the average crystallite size (D) for the NiNPs, as shown in Eq. 1.

$$D = \frac{0.89\lambda}{\mathrm{B}\cos\theta} \tag{1}$$

where B denotes full-width half-maximum, λ stands for wavelength (0.15418 nm), and θ represents Bragg angle of XRD peak.

The raw MWCNTs in Fig. 2b revealed low-intensity diffraction peak at angles 2θ = 26.35°. In comparison, the functionalized MWCNTs exhibited a very intense diffraction peak at the angles 2θ = 26.3° and 25.97° (002) and 42.31° indexed to the (002) and (101) lattice plane reflections of graphite-like materials characteristic of CNTs. The peak intensity indicated highly improved crystallinity, confirming the attachment of the oxygen-containing covalent functional groups on the MWCNTs walls (Cao et al. 2003; Li et al. 2011). The XRD diffractogram of NiPcMWCNTs nanocomposite, as depicted in Fig. 2c, shows eight peaks at 2θ = 6.92°, 10.97°, 15.08°, 17.06°, 26.26°, 44.64°, 52.02° and 76.60°. The eclectic and strong peak at 26.26° (002) is assigned to the fMWCNTs, while 44.64°, 52.02°, and 76.60° are attributed to NiNPs. The remaining peaks (6.92°, 10.97°, 15.08°, and 17.07°) are distinctive peaks of phthalocyanine (Cao et al. 2003; Li et al. 2011).

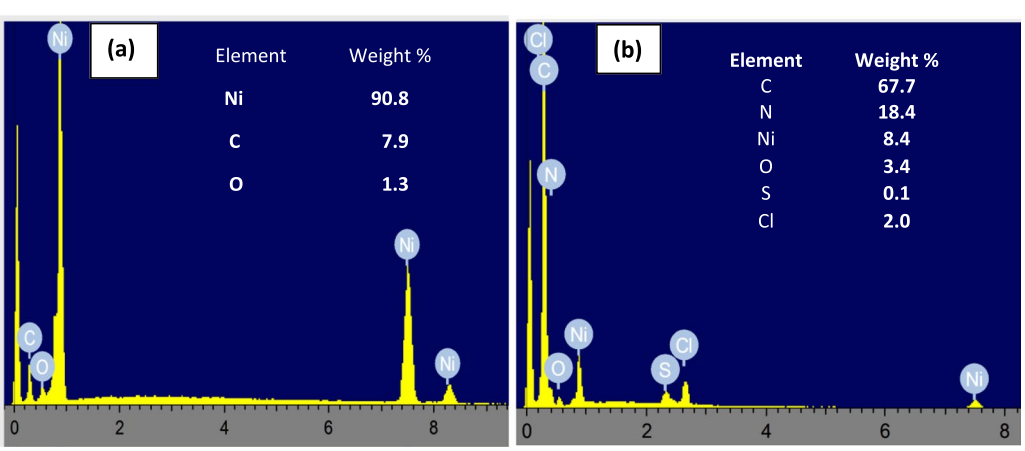

Fig. 1 EDX spectra of **a** NiNPs, **b** NiPcMWCNTs

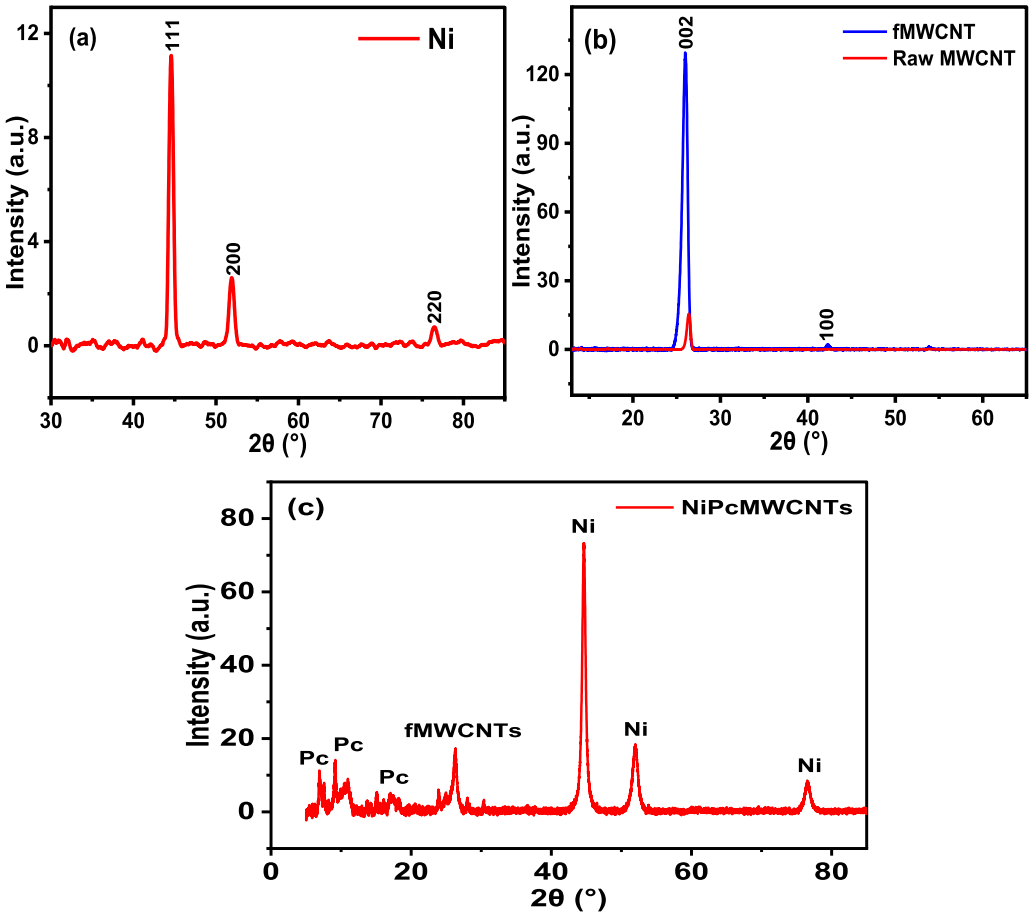

Fig. 2 XRD patterns of **a** NiNPs, **b** fMWCNTs and rMWCNTs, and **c** NiPcMWCNTs nanocomposite

Scanning *electron microscopy* (SEM)

The SEM images of the nanomaterials and the nanocomposite are depicted in Fig. 3a–d. A smooth spherical particle shape but irregular particle morphology with a grain size of 18 nm was observed for NiNPs's TEM image in Fig. 3a. The value is more in line with the result obtained by applying Scherrer's equation. The micrograph (Fig. 3d) displays NiNPs and Pc attaching to the fMWCNTs surface, thereby suggesting a successful NiPcMWCNTs nanocomposite fabrication.

Ultraviolet–visible characterization

The UV–visible spectra of (a) nickel nanoparticles (b) Phthalocyanine (c) raw MWCNTs & functionalized MWCNTs, and (d) NiPcMWCNTs nanocomposite are illustrated in Fig. 4. Figure 4a represents the NiNPs spectrum with a prominent peak at 296 nm. The UV–visible spectrum of rMWCNTs and fMWCNTs, as depicted in Fig. 4b shows that the absorption peaks at 289 nm (rMWCNTs) and 294 nm (fMWCNTs) differ noticeably, which confirms that the rMWCNTs were successfully functionalized.

Two predominant peaks are peculiar with Phthalocyanine: the Q-band and the B-band. The Q-band takes place at 668 nm as a result of the electronic transitions from the lowest unoccupied molecular orbital to the highest occupied molecular orbital ($\pi \rightarrow \pi^*$ transition), while the B-band takes place in the ultraviolet region between 310–400 nm due to the transition from π^* to π. At a wavelength of 668 nm, there was Q-band splitting in the phthalocyanine spectrum due to the compound's D_{2h} symmetry. A similar Q-band splitting is observed in the NiPcMWCNTs nanocomposite spectrum (Fig. 4d), which includes all the identified peaks for Pc, NiNPs, and fMWCNTs.

Electrochemical characterization

To investigate the electron transport behaviors of nanomaterials and the nanocomposite, the electrochemical characterization of all the electrodes was carried out using CV. All the electrodes produced a pair of redox

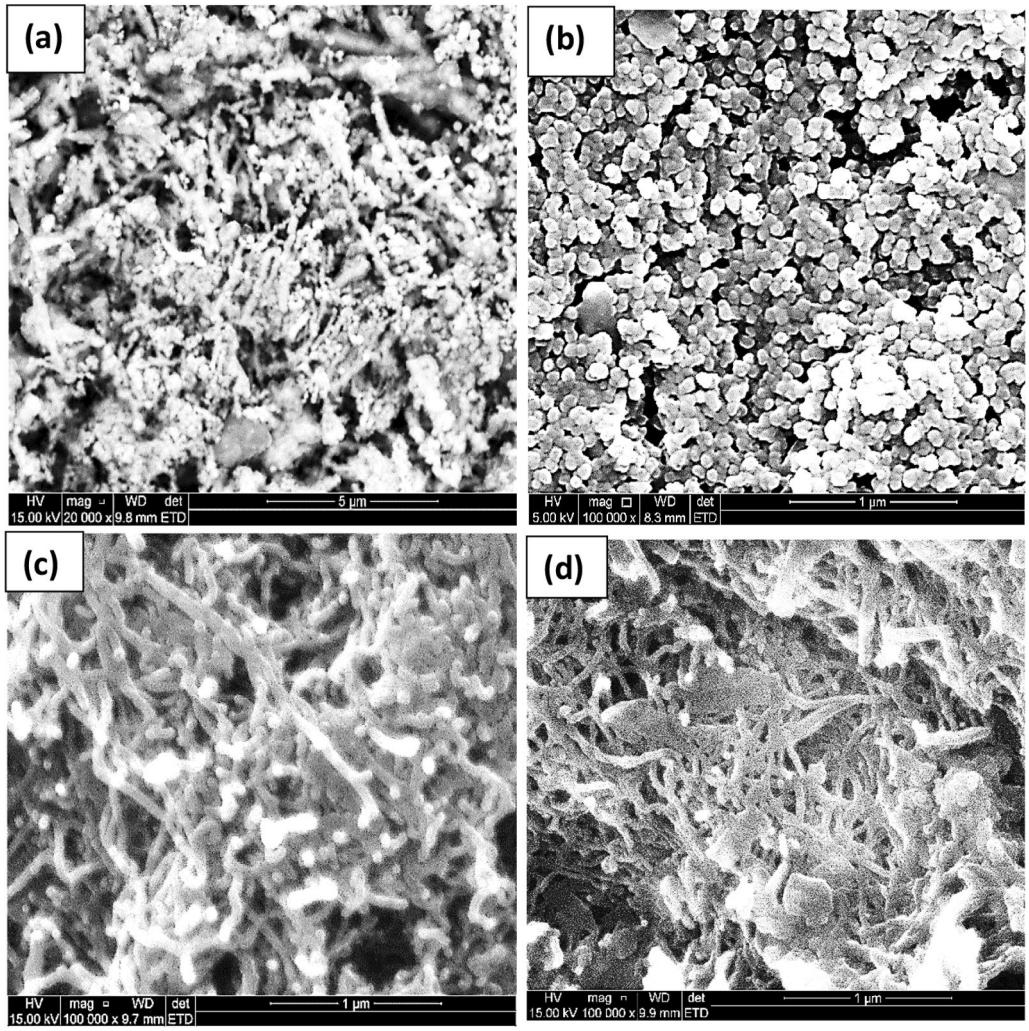

Fig. 3 SEM images of **a** NiNPs, **b** Pc, **c** fMWCNTs, and **d** NiPcMWCNTs nanocomposite

peaks in 5 mM $K_3(Fe(CN)_6/K_4(Fe(CN)_6$ made in 0.1 M of PBS (pH 7) at 25 mVs^{-1}, as displayed in the cyclic voltammograms (Fig. 5). According to Table 1, the values of the peak separation (Ep) obtained for the electrodes were GCE (0.39 V), Pc/GCE (0.25 V), Ni/GCE (0.18 V), fMWCNTs/GCE (0.13 V), and NiPcMWCNTs/GCE (0.18 V). The Ep values obtained are greater than 59 mV predicted for rapid one-electron transport, indicating a quasi-reversible process at the electrode surfaces (Haque et al. 2013; Zangeneh Kamali et al. 2014). Table 1 further demonstrates that all electrodes' Ipa/Ipc values are about equal to one. This implies reversibility on all modified electrode surfaces, including the bare electrode. Figure 5 shows the relative current responsiveness of each electrode, with NiPcMWCNTs/GCE (457.0 µA) coming in first place, followed by fMWCNTs/GCE (58.0 µA), Ni/GCE (35.6 µA), Pc/GCE (21.5 µA), and GCE (25.0 µA). An anodic peak current (Ipa) of 457.0 µA, roughly 18 times more than GCE's peak current and about 8 times more than other modified electrodes, was recorded for the NiPcMWCNTs/GCE modified electrode. This suggests that the NiPcMWCNTs/GCE electrode offers the greatest current response of all the electrodes. The combined cooperative effect of fMWCNTs, NiNPs, and Pc is responsible for the improved current response displayed at the NiPcMWCNTs/GCE electrode. This effect is brought on by the phthalocyanine and fMWCNTs sizable surface area, as well as the fMWCNTs and nickel nanoparticles high electrical conductivity (Mphuthi et al. 2017).

Equally, the electrodes' specific capacitance (Sc) was calculated from the individual voltammograms of the modified electrodes using Eq. 2. Noteworthy, a larger capacitive current was exhibited by the NiPcMWCNTs/GCE in comparison to the other electrodes, indicating its superiority in charge and discharge capacity over them.

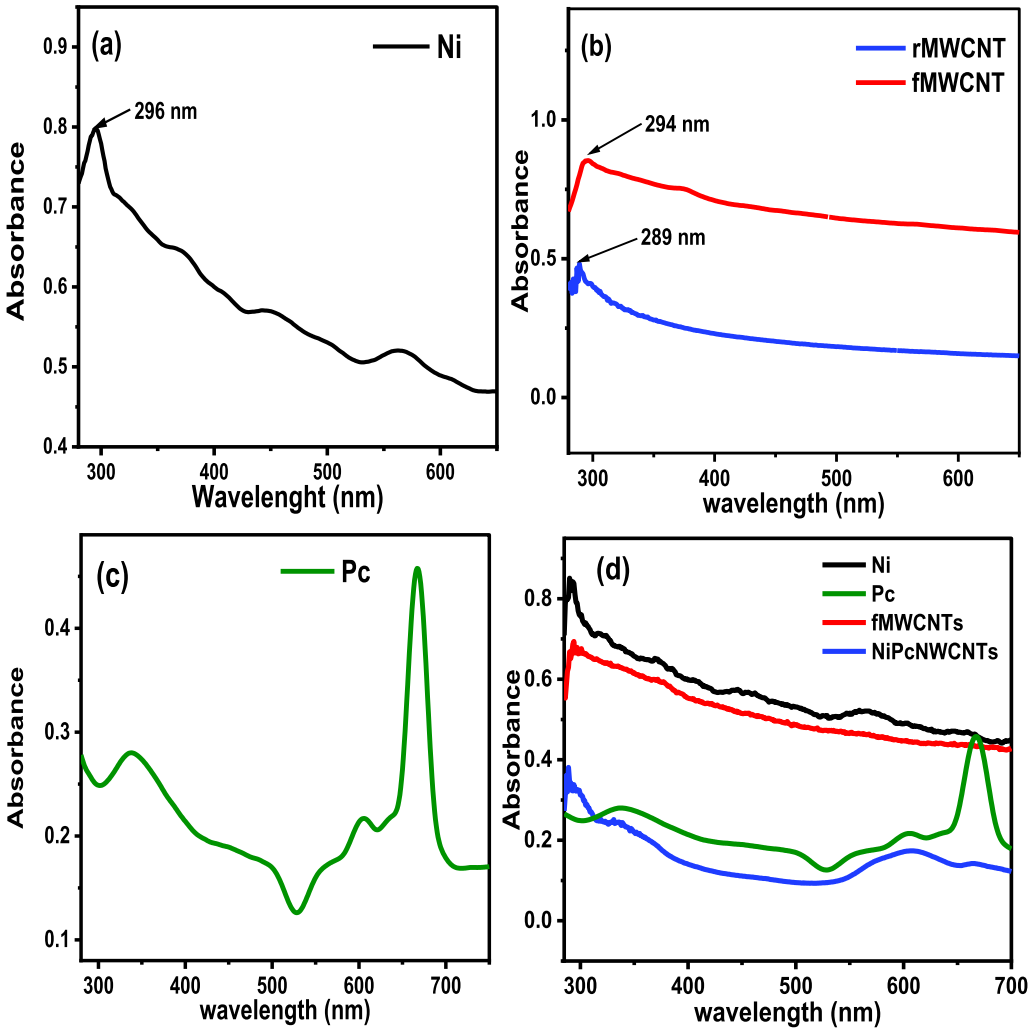

Fig. 4 UV–visible spectra for **a** NiNPs, **b** fMWCNTs and rMWCNTs, **c** Pc, and **d** NiNPs, fMWCNTs, Pc, and NiPcMWCNTs nanocomposites

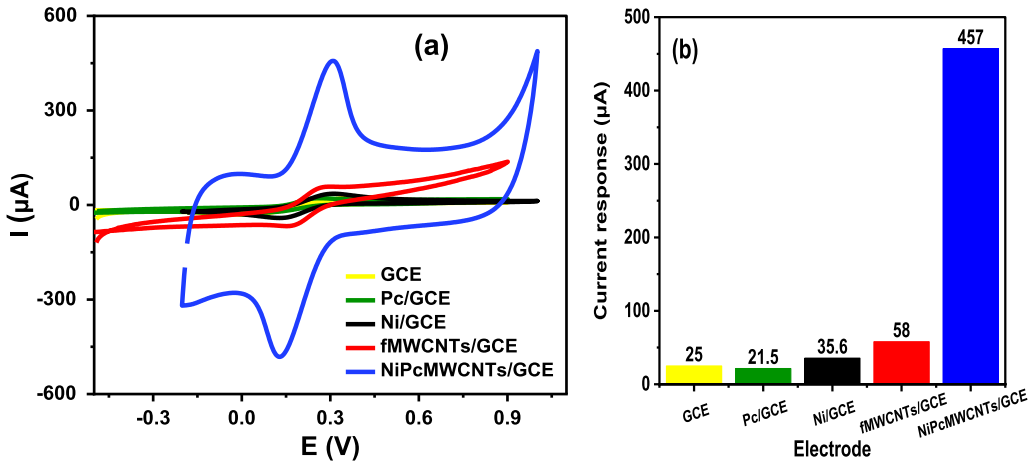

Fig. 5 **a** Cyclic voltammograms of the electrodes in 5 mM $K_3(Fe(CN)_6/K_4(Fe(CN)_6$ made in 0.1 M of PBS at 25 mV s^{-1}, and **b** Histogram of the current responses for GCE, Pc/GCE, Ni/GCE, fMWCNTs/GCE, and NiPcMWCNTs/GCE electrodes

Table 1 Cyclic voltammetry data of all the electrodes in 5 mM $K_3(Fe(CN)_6/K_4(Fe(CN)_6$ made in 0.1 M of PBS (pH 7)

Working electrode	I_{pa} (μA)	I_{pc} (μA)	I_{pa}/I_{pc}	E_{pa} (V)	E_{pc} (V)	ΔEp (V)	E° (V)	Sc (F/g)
Bare GCE	25.0	−30.0	−0.83	0.40	0.01	0.39	0.20	0.17
Pc/GCE	21.5	−25.9	−0.83	0.26	0.01	0.25	0.13	0.26
Ni/GCE	35.6	−41.3	−0.86	0.31	0.13	0.18	0.09	0.31
fMWCNTs/GCE	58.0	−67.1	−0.87	0.29	0.16	0.13	0.07	0.63
NiPcMWCNTs/GCE	457.0	−482.0	−0.95	0.31	0.13	0.18	0.09	6.80

GCE, Bare glassy carbon electrode; Pc/GCE, Phthalocyanine/glassy carbon electrode; Ni/GCE, Nickel/glassy carbon electrode; fMWCNTs/GCE, Functionalized multi-walled carbon nanotubes/glassy carbon electrode; NiPcMWCNTs/GCE, Nickel phthalocyanine multi-walled carbon nanotubes/glassy carbon electrode

$$Sc = \frac{A}{2mk(V_2 - V_1)} \quad (2)$$

where A denotes the area of CV curve (AV), m denotes the mass of active material (g), k stands for scan rate (mV s^{-1}), and $(V_2 - V_1)$ symbolizes the potential window (V s^{-1}).

In reference to Table 1, the Sc values of the electrodes were 0.17 F g^{-1} (GCE), 0.26 F g^{-1} (Pc/GCE), 0.31 F g^{-1} (Ni/GCE), 0.63 F g^{-1} (fMWCNTs/GCE), and 6.80 F g^{-1} (NiPcMWCNTs/GCE). This data makes it evident that NiPcMWCNTs/GCE offered a substantially greater Sc compared to the other electrodes. The enhanced capacitive performance demonstrated by the NiPcMWCNTs/GCE has also been accredited to the Phthalocyanine and fMWCNTs sizable surface area, as well as the fMWCNTs and nickel nanoparticles high electrical conductivity. These electrodes' capacitive properties were further investigated using the EIS method.

Scan rate study

The impact of scan rate variation (25–300 mV s^{-1}) on the electrochemical processes occurring on the surface of the NiPcMWCNTs/GCE electrode was studied in a solution of 5 mM $K_3(Fe(CN)_6/K_4(Fe(CN)_6$ made in 0.1 M of PBS. An increase in the scan rate is precisely proportional to the peak currents, as seen in Fig. 6a. The plot of the scan rate's square root vs peak current in Fig. 6b, shows a linearity, resulting in the regression equation below.

$$I_{pa} = 0.0054\, v^{1/2} - 0.0004 \qquad (R^2 = 0.9987)$$
$$I_{pc} = 0.0048\, v^{1/2} + 0.0003 \qquad (R^2 = 0.9990)$$

The linear connection between the scan rate's square root and the peak currents suggests a common diffusion-controlled mechanism for the NiPcMWCNTs/GCE.

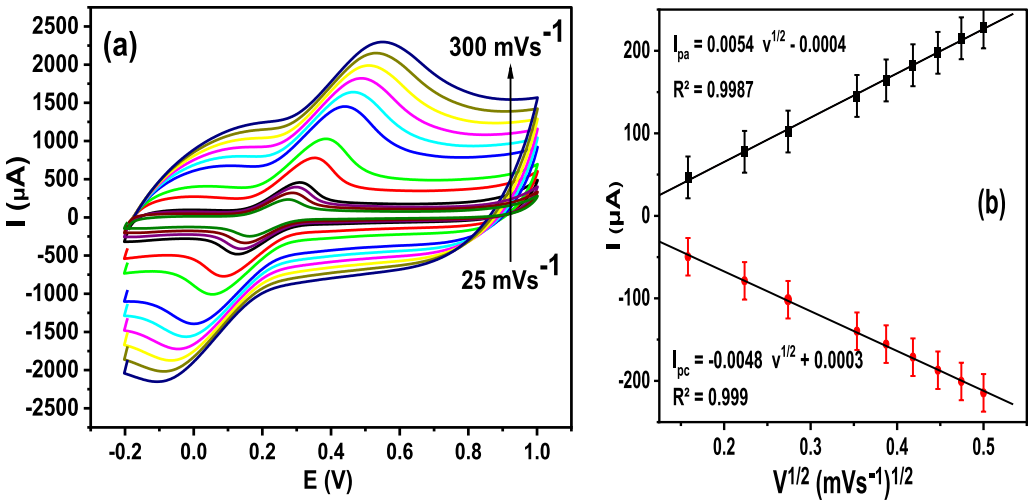

Fig. 6 Cyclic voltammogram of **a** NiPcMWCNTs/GCE from 25 to 300 mV s^{-1} in 5 mM $K_3(Fe(CN)_6/K_4(Fe(CN)_6$ made in 0.1 M of PBS, and **b** linear plot of scan rate's square root vs peak current

Electrochemical impedance spectroscopy (EIS) study

To fully examine the capacitive properties and the electron transport behaviours of these electrodes, an EIS study was performed in 5 mM $K_3(Fe(CN)_6/K_4(Fe(CN)_6$ made in 0.1 M of PBS (pH 7) via a Metrohm Autolab Potentiostat. Having 0.3 V as its constant potential against Ag/AgCl, saturated with 3 M KCl, with an operating frequency of 100 kHz–0.1 Hz. The experiment was conducted at 0.3 V since it had the highest peak current and capacitance at this potential. Figure 7 displays the Nyquist plots for the fitted data of the electrodes in 5 mM $K_3(Fe(CN)_6/K_4(Fe(CN)_6$ made in 0.1 M of PBS, While X denotes the circuit employed to fit the obtained data. The circuit's components contain the following parameters: Capacitance (C), constant phase element (CPE), solution resistance (R_s), charge transfer resistance (R_{ct}), and warburg impedance (W). Table 2 provides the obtained EIS fitted data along with individual chi-square (x^2) values. The EIS data were well fitted, as evidenced by the small % errors in the parentheses and the negative x^2 values obtained.

The R_{ct} values recorded for the electrodes as presented in Table 2, were NiPcMWCNTs/GCE (0.18), fMWCNTs/GCE (0.44), Pc/GCE (0.89), Ni/GCE (1.39), and GCE (8.73 KΩ) with the NiPcMWCNTs/GCE having the lowest R_{ct}, indicating its rapid electrons transport capability over other electrodes. The NiPcMWCNTs/GCE fast electron transfer ability is due to the functionalized MWCNTs' high conductivity, which serves as an excellent electron conductor between Pc and NiNPs and the NiPcMWCNTs/GCE's surface. The reduction in R_{ct} values of the modified electrodes, suggests that the bare electrode was properly modified with the nanocatalysts. The result obtained here is similar to the current response result in the CV. This also led to the huge Sc values obtained by the modified electrodes, particularly the NiPcMWCNTs/GCE. The n values of all the electrodes, which range from 0.72 to 0.97, may be responsible for the easy diffusion of ions across the solution/electrode interface.

Choice of electrolyte

Prior to the detection of bromate, an impedance spectroscopy experiment was carried out in four dissimilar

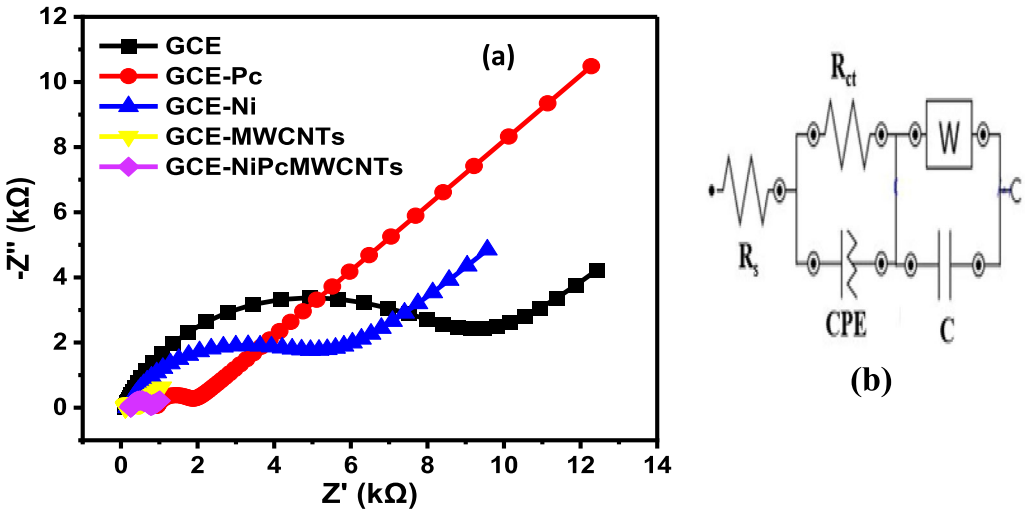

Fig. 7 Nyquist plots of the electrodes in **a** 5 mM $K_3(Fe(CN)_6/K_4(Fe(CN)_6$ made in 0.1 M of PBS and **b** Circuit employed to fit the obtained EIS data

Table 2 Overview of the fitted EIS parameters of the electrodes

Impedance spectroscopy parameter (the percentage errors are in parentheses)						
Electrode	**R_s (Ω)**	**R_{ct} (Ω)**	**CPE (μF)**	**W (F)**	**N**	**X^2**
Bare GCE	110 (3.78)	8.73 (5.31)	3.80 (16.7)	226 (1.84)	0.80 (1.26)	0.555
Pc/GCE	928 (4.42)	0.89 (8.60)	0.16 (79.6)	85.1 (2.44)	0.86 (9.30)	0.357
Ni/GCE	301 (2.03)	1.39 (3.43)	6.70 (16.3)	524 (4.46)	0.72 (2.91)	0.215
fMWCNTs/GCE	85 (2.32)	0.44 (5.99)	2644 (29.9)	67 (3.31)	0.97 (12.9)	0.164
NiPcMWCNTs/GCE	104 (0.94)	0.18 (5.60)	27.2 (4.85)	148 (9.70)	0.72 (0.94)	0.507

GCE, Bare glassy carbon electrode; Pc/GCE, Phthalocyanine/glassy carbon electrode; Ni/GCE, Nickel/glassy carbon electrode; fMWCNTs/GCE, Functionalized multi-walled carbon nanotubes/glassy carbon electrode; NiPcMWCNTs/GCE, Nickel phthalocyanine multi-walled carbon nanotubes/glassy carbon electrode

supporting electrolytes with NiPcMWCNTs/GCE. This study was done to ascertain the most suitable supporting electrolyte for bromate detection. The four electrolytes investigated were 0.1 M sodium acetate buffer (SAB) containing 0.1 M $KBrO_3$ (pH 7), 0.1 M Na_2SO_4 containing 0.1 M $KBrO_3$ (pH 2), 0.1 M H_2SO_4 containing 0.1 M $KBrO_3$ (pH 1), and 0.1 M PBS containing 0.1 M $KBrO_3$ (pH 7). Figure 8 depicts the Nyquist plot of NiPcMWCNTs/GCE in H_2SO_4, SAB, PBS, and Na_2SO_4 supporting electrolytes. The R_{ct} values obtained for the NiPcMWCNTs/GCE in the four supporting electrolytes were 0.06, 0.36, 1.98, and 9.04 kΩ for the H_2SO_4, SAB, PBS, and Na_2SO_4, respectively (as shown in Table 3). The lowest R_{ct} value obtained for NiPcMWCNTs/GCE was in H_2SO_4 electrolyte, while the highest was in Na_2SO_4. This indicates that the H_2SO_4 electrolyte is a better medium for the rapid transfer of electrons than the other electrolytes investigated.

The results of the EIS of the NiPcMWCNTs/GCE in the four dissimilar electrolytes show that the nanocomposite electrode is a suitable bromate sensor, particularly in the H_2SO_4 electrolyte. A lot of studies on the usage of H_2SO_4 for bromate detection have been reported in the literature (Ding et al. 2014; Hassan et al. 2013; Majidi et al. 2015; Zhang et al. 2020). Hence, the fast electron transport capability of the nanocomposite electrode in the H_2SO_4 electrolyte accounted for its choice as the suitable electrolyte for bromate detection.

Electroanalysis of bromate at NiPcMWCNTs/GCE

Utilizing cyclic voltammetry, the electrocatalytic property of bromate in 0.1 M H_2SO_4 (pH 1) containing 1 mM $KBrO_3$ at 25 mV/s was investigated. The cyclic voltammograms (CV) of the electrodes are depicted in Fig. 9a. Expectedly, the NiPcMWCNTs/GCE has the highest reduction peak current. This supports the finding that NiPcMWCNTs/GCE is superior to all other electrodes. In comparison with other electrodes, the NiPcMWCNTs/GCE displayed a better potential and a well-defined bromate cathodic (reduction) peak current. From Table 4, the bromate reduction potential (E_{pc}) and current (I_{pc}) recorded for the NiPcMWCNTs/GCE, fMWCNTs/GCE, Ni/GCE, Pc/GCE, and GCE are −1299.10 μA (−0.0430 V), −306.59 μA (−0.2208 V), −11.78 μA (−0.2978 V), −36.70 μA (−0.3124 V), and −23.19 μA (−0.2332 V), respectively. In addition to the reduction

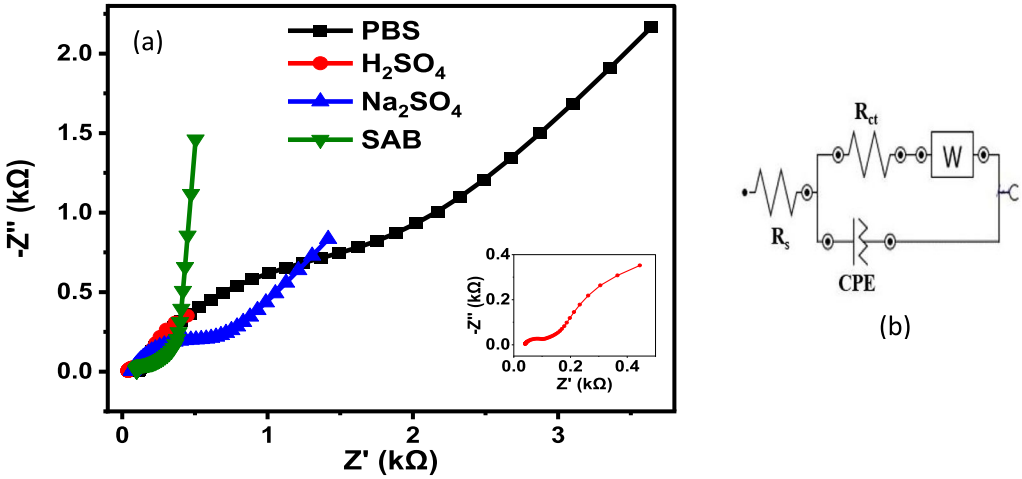

Fig. 8 Nyquist plots of **a** NiPcMWCNTs/GCE in H_2SO_4, PBS, Na_2SO_4, and SAB electrolyte, and **b** circuit employed to fit the obtained EIS data

Table 3 EIS results of NiPcMWCNTs/GCE in four dissimilar electrolytes

EIS parameter						
Electrolyte	**R_s (Ω)**	**CPE (μF)**	**R_{ct} (kΩ)**	**W (μF)**	**N**	**X^2**
H_2SO_4	39.9 (2.95)	42.0 (53.2)	0.06 (9.53)	3130 (3.96)	0.79 (8.22)	0.320
Na_2SO_4	62.6 (1.96)	17.8 (8.06)	9.04 (21.8)	37.5 (5.88)	0.78 (1.49)	0.186
PBS	105 (2.20)	43.4 (10.65)	1.98 (7.21)	407 (5.98)	0.63 (2.38)	0.164
SAB	91 (2.50)	306 (11.5)	0.36 (5.12)	714 (5.70)	0.50 (3.68)	0.192

H_2SO_4, Sulfuric acid; Na_2SO_4, Sodium sulphate; PBS, Phosphate buffer solution; SAB, Sodium acetate buffer

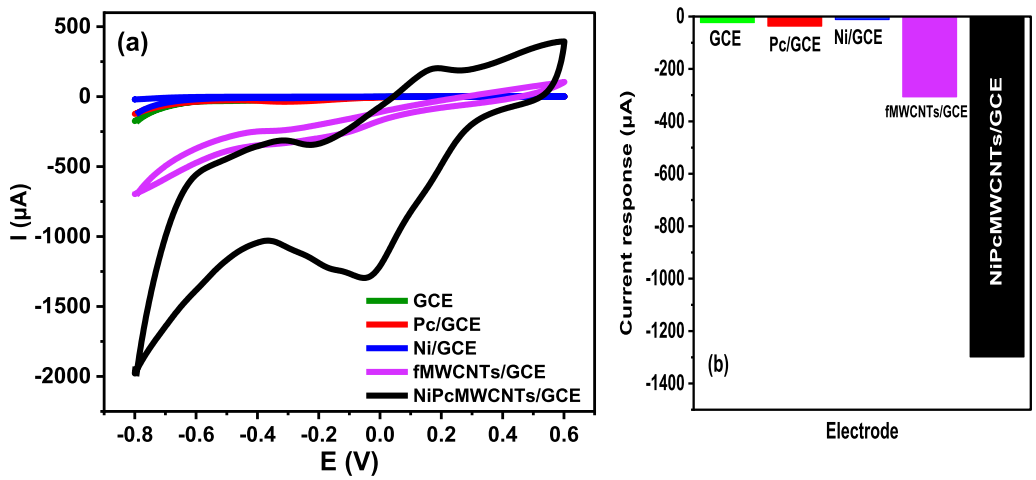

Fig. 9 Cyclic voltammogram of the electrodes in **a** 1 mM $KBrO_3$ prepared in 0.1 M H_2SO_4 (pH 1) and **b** histogram of the electrodes' current response

Table 4 Summary of CV results of the electrodes in 1 mM $KBrO_3$ prepared in 0.1 M H_2SO_4 (pH 1) at 25 mV/s

Working electrode	I_{pc} (μA)	E_{pc} (V)	I_{pa} (μA)	E_{pa} (V)
Bare GCE	−23.19	−0.2332		
Pc/GCE	−36.70	−0.3124		
Ni/GCE	−11.78	−0.2978		
fMWCNTs/GCE	−306.59	−0.2208		
NiPcMWCNTs/GCE	−1299.10	−0.0430	203.20	0.1795

GCE, Bare glassy carbon electrode; Pc/GCE, Phthalocyanine/glassy carbon electrode; Ni/GCE, Nickel/glassy carbon electrode; fMWCNTs/GCE, Functionalized multi-walled carbon nanotubes/glassy carbon electrode; NiPcMWCNTs/GCE, Nickel phthalocyanine multi-walled carbon nanotubes/glassy carbon electrode

(cathodic) peak demonstrated by all of the electrodes, the modified NiPcMWCNTs/GCE also displayed an anodic peak, as seen in Fig. 9; however, this peak vanishes at higher scan rates. The NiPcMWCNTs-GCE outperformed other electrodes in terms of electrocatalytic response for bromate reduction.

The good electronic conductivity of nanocomposite components (Pc, NiNPs, and fMWCNTs), their biocompatibility with the bromate, and their large surface area are responsible for this improved current response. Remarkably, a visible bromate reduction peak given by NiPcMWCNTs/GCE resulted from the electron transfer that happened quickly during the bromate reduction process.

Impact of scan rate variation

The impact of varied scan rate at NiPcMWCNTs/GCE in 0.1 M H_2SO_4 solution containing 1 mM bromate was examined with CV. An increment from 25 to 300 mV/s, gradually increased the cathodic peak current with a positive shift of the peak potentials, as shown in Fig. 10a. A linear connection exists between the scan rate's square root and the cathodic peak current, giving a linear regression (Eq. 3). Thereby, suggesting that the NiPcMWCNTs/GCE reduction process is a diffusion-controlled process (Wierzbicka and Sulka 2016).

$$I_{pc} = -1.283E-04\,v^{1/2} - 6.7592E-4 \qquad \left(R^2 = 0.9899\right) \tag{3}$$

$$E_{pc} = -0.27133 + 0.32003\ \log v \qquad \left(R^2 = 0.99849\right) \tag{4}$$

A linear connection also exists between the logarithm of the scan rate (50–175 mV s^{-1}) and the peak potential, as depicted in Fig. 10d, with a linear equation represented in Eq. 4. Using the Laviron equation, given that the slope of the graph of log v against E_{cp} is b1 (Eq. 5), the electron transfer coefficient (α), as well as the number of electrons transferred (n), can then be calculated.

$$b1 = \frac{\mathrm{RT}}{\propto \mathrm{nF}} \tag{5}$$

$$E_p = \frac{\mathrm{b}}{2}\log v + K \tag{6}$$

where n, F, R, K, α, *v*, and T denote the number of electrons in cathodic reaction, Faraday constant (96,485 C mol^{-1}), universal gas constant (8.314 J K^{-1} mol^{-1}), reaction rate constant, electron transfer coefficient, potential scan rate, and temperature Kelvin.

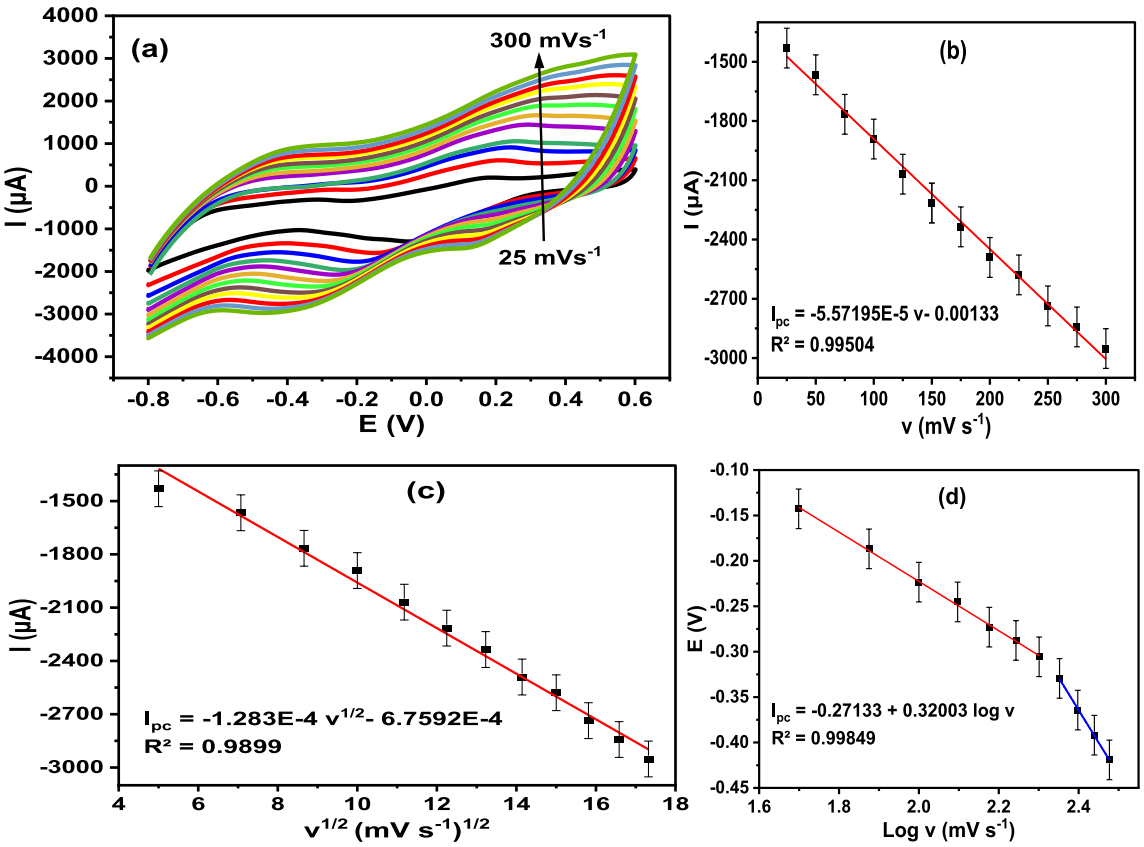

Fig. 10 Cyclic voltammogram of **a** NiPcMWCNTs/GCE (25–300 mV s^{-1}) in 1 mM $KBrO_3$ prepared in 0.1 M H_2SO_4 (pH 1), **b** linear graph of scan rate against cathodic peak current I_{pc}, **c** linear graph of scan rate's square root against cathodic potential I_{pc}, and **d** linear graph of logarithm of scan rate against cathodic potential E_{pc}

$$Ni^{II}Pc \longrightarrow Ni^{III}Pc + e^-$$

$$6Ni^{III}Pc + BrO_3^- + 6H^+ \longrightarrow 6Ni^{II}Pc + Br^- + 3H_2O$$

Scheme 1 Mechanism of bromate reduction

The Tafel slope b is calculated as 225 mV dec^{-1} from Eq. 6. A Tafel slope obtain within the range of 60–120 mV dec^{-1} suggests a one-electron process at the rate-determining step, while a Tafel slope greater than 120 mV dec^{-1} suggests an adsorptive process at the electrode surface (Ndebele et al. 2021). The strong binding force between the electrode modifier and the analyte has been attributed as the cause of this kind of adsorption (Fang and Liu 2014). The Tafel slope for bromate reduction (225 mV dec^{-1}) is larger than 120 mV dec^{-1} implying the occurrence of an adsorptive process at NiPcMWCNTs/GCE electrode (Ndebele et al. 2021). The proposed mechanism of bromate reduction at NiPcMWCNTs/GCE, as illustrated in Scheme 1, involves two phases. The first phase is the oxidation of $Ni^{II}Pc$ to $Ni^{III}Pc$, while the second phase is the reduction of bromate to bromide and $Ni^{II}Pc$ regeneration.

Effects of pH

Using CV in 0.1 M H_2SO_4 solution at varied pH values (1, 2, 3, & 5), the effect of the varied electrolyte pH on the electrochemical performance of NiPcMWCNTs/GCE towards bromate reduction was investigated. The primary goal of this investigation was to attain the best reduction peak resolution for bromate detection. With an increasing pH of the electrolyte, a negative shift in the cathodic peak potentials was noticed, suggesting that the electrocatalytic reduction of bromate involves proton transfer at the modified nanocomposite electrode. The highest cathodic peak current of bromate was attained at the pH of 1 and subsequently reduced with increasing pH. For this reason, a pH of 1 was used throughout the experiment. Interestingly, the electroanalysis of bromate

at a pH of 1 has been widely reported (Li et al. 2006, Zhou et al. 2012).

Concentration studies

EIS detection of bromate at NiPcMWCNTs/GCE

The use of NiPcMWCNTs/GCE for bromate detection was favoured among other electrodes due to its lower R_{ct} value and higher current response. EIS technique was adopted for BrO_3^- detection at the developed sensor. Figure 11a shows the Nyquist plot of NiPcMWCNTs/GCE in 24–100 μM BrO_3^-. Expectedly, as the BrO3 concentration increases, the charge-transfer resistance R_{ct} reduces. The charge-transfer resistance and BrO_3^- concentration were found to be linearly related over a concentration range of $2.4\times10^{-5}-1.0\times10^{-4}$ μM for NiPcMWCNTs/GCE (Fig. 11b). The LoD and LoQ for BrO_3^- for NiPcMWCNTs/GCE were calculated using Eq. 7 and 8, respectively.

$$LoD = \frac{3.3\delta}{m} \tag{7}$$

$$LoQ = \frac{10\delta}{m} \tag{8}$$

where δ denotes the standard deviation of the intercept, m represents the slope of the intercept.

The LoD and LoQ obtained for the NiPcMWCNTs/GCE were 6.72 μM and 20.38 μM, respectively, with a sensitivity of 483.7 μM Ω^{-1}. The LoD obtained for the fabricated sensor is compared in Table 5 with other reported bromate sensors in the literature.

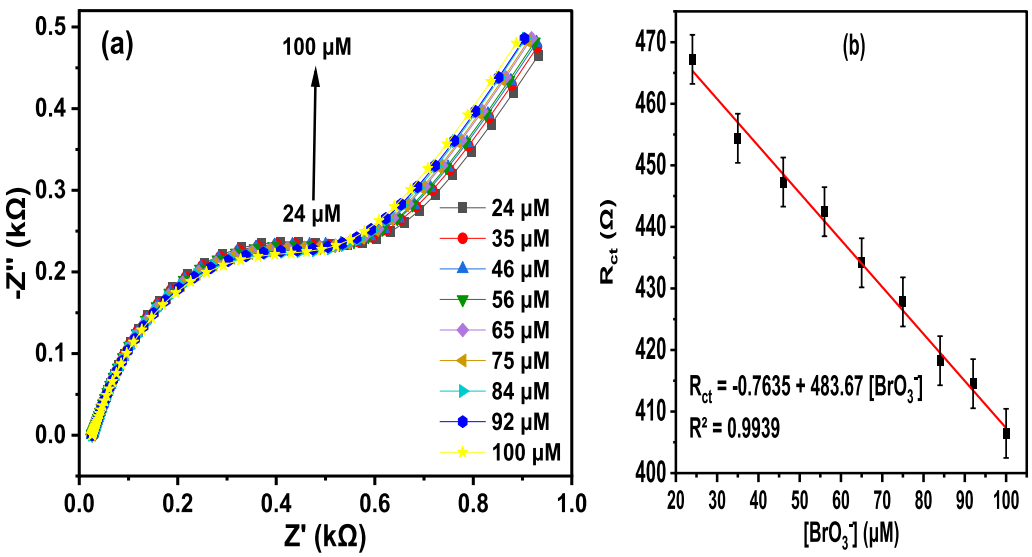

Fig. 11 Nyquist plot of **a** NiPcMWCNTs/GCE over BrO_3^- concentration range of 24–100 μM at pH 1. **b** plot of R_{ct} versus concentration

Table 5 Comparison of the proposed sensor with the previous bromate sensors

Electrode	Technique	LoD (μM)	LDR (μM)	Sensitivity (μA μM^{-1})	References
NENU-3 film	AP	12	50–19,100	11.2	Shi et al. (2016)
Nafion/Hb/FeS@MoS_2-C/CILE	CV	1	50–25,000		Zhang et al. (2022a, b)
PTh-D/nafion/AuE	ECL	1	1–100,000	108.41	Li et al. (2014)
$CoW_{11}Co/PVP/TiO_2$/GCE	CV	5	20–4400	–	Li et al. (2005)
NiPcMWCNTs/GCE	SWV	1.47	12–56	1293.0	This work
NiPcMWCNTs/GCE	EIS	6.72	24–100	483.7	This work

NENU-3 film, Electroactive metal–organic framework film; Nafion/Hb/FeS-MoS_2-C/CILE, Petal-shaped FeS@MoS_2-C nanocomposite uniformly dispersed nanocomposite, hemoglobin (Hb) and Nafion mixture prepared carbon ionic liquid electrode (CILE); PTh-D/nafion/AuE-poly[3-(1,1′-dimethyl-4-piperidinemethylene) thiophene-2,5-diylchloride] (PTh-D); and $CoW_{11}Co/PVP/TiO_2$/GCE, tetrabutyammonium cobalt (III) 12-tungsten poly (4-vinylpyridine)(PVP) in a TiO_2 sol–gel matrix

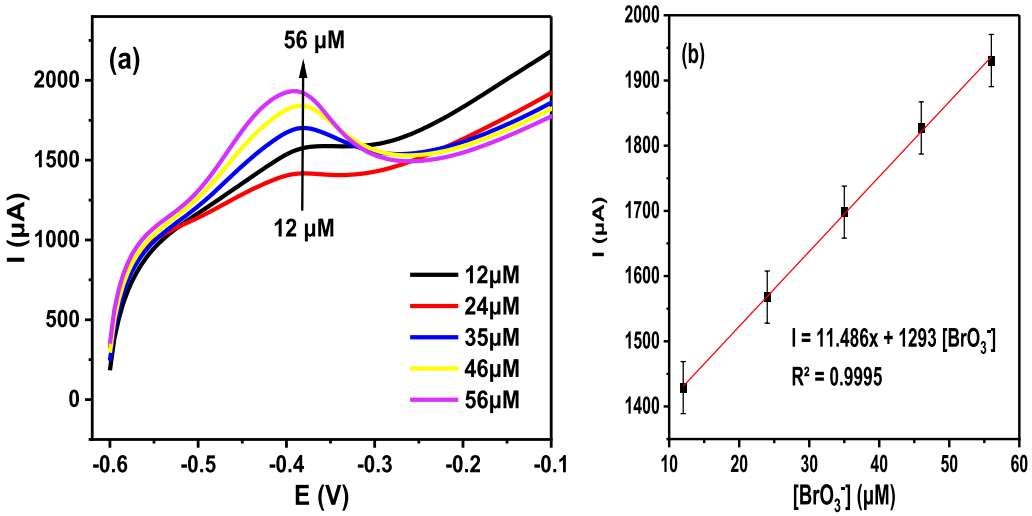

Fig. 12 Square wave voltammograms of **a** NiPcMWCNTs-GCE over BrO_3^- concentration range of 12–56 µM at pH 1, and **b** plot of current versus concentration obtained from (**a**)

SWV detection of bromate at NiPcMWCNTs/GCE

At the NiPcMWCNTs/GCE electrode, the electrocatalytic reduction of BrO_3^- was further examined via the square wave voltammetry (SWV) technique. The voltammogram of NiPcMWCNTs/GCE in the bromate concentration range of 12–56 µM is depicted in Fig. 12a. Here, the peak current also increased with the BrO_3^- concentration. The current response and BrO_3^- concentration were found to be linearly related, as depicted in Fig. 12b. At the developed sensor, there is a linear relationship between the BrO_3^- concentration and the current over an LDR of 12 to 56 µM.

The developed sensor's LoD and LoQ were estimated as 1.47 and 4.46 µM, respectively. Compared to the EIS results, the LoD and LoQ achieved using SWV are superior. Additionally, the sensor has an extremely high sensitivity (1293 µA μM^{-1}).

Interference studies

One of the qualities of a good sensor is its ability to selectively detect the target analyte amidst the likely interfering ions in a real sample. As a result, the performance of the developed sensor is examined in relation to several potential interfering species. The selectivity of the NiPcMWCNTs/GCE towards bromate detection was investigated through EIS technique. The interference study was accomplished by comparing the EIS response (R_{ct} value) of 0.1 mM bromate in 0.1 M H_2SO_4 solution before and after adding certain concentrations of the interfering ions to a known bromate concentration at a voltage of − 0.3. The Nyquist plot (not shown) demonstrates no change in the R_{ct} value of bromate concentration with the addition of the interfering ions concentration except for a few ions. The difference between the R_{ct} obtained in 0.1 mM bromate alone, and the R_{ct} of the mixture of interfering ion concentration plus 0.1 mM bromate serves as a basis for the sensor selectivity. As depicted in Table 6, the addition of tenfold excesses of these species (K^+, Na^+, SO_4^{2-}, CO_3^{2-}, ClO_3^-, and Cl^-) does not affect the R^{ct} value of the bromate, except for IO_3^- and Mg^{2+} that show a slight degree of interference. There was about 2.2% and 3.2% drop in R_{ct} value of the proposed sensor upon the addition of IO_3^- and Mg^{2+}. The IO_3^{2-} reacts and undergoes oxidation in the H_2SO_4 solution, which is mainly responsible for its interference. The interference caused by Mg^{2+} is possibly due to the precipitates formed by the Mg^{2+} in the electrolyte solution.

Table 6 Impact of interfering ions on bromate detection at NiPcMWCNTs/GCE

Interfering species	Initial R_{ct} (Ω)	Final R_{ct} (Ω)	% Drop of R_{ct}
K^+	452.76	452.76	Nil
Cl^-	452.76	452.76	Nil
CO_3^{2-}	452.76	452.76	Nil
ClO_3^-	452.76	452.76	Nil
Na^+	452.76	452.70	0.01
SO_4^{2-}	452.76	452.62	0.03
IO_3^-	452.76	446.36	1.4
Mg^{2+}	452.76	470.25	3.9

K^+, Potassium ion; Cl^-, Chloride ion, CO_3^{2-}, Carbonate ion; ClO_3^-, Chlorate ion; Na^+, Sodium ion; SO_4^{2-}, Sulphate ion; IO_3^-, Iodate ion; and Mg^{2+}, Magnesium ion

Real sample analysis

Prior to the analysis of the real samples, a preliminary qualitative test was carried out on a small portion of the bread samples by adding a few drops of a mixture of 1 mL of 0.5 M hydrochloric acid and 5 mL of 0.05 M promethazine solution. When the bread sample solution changes to pink, it confirms that bromate is present. This preliminary qualitative test is important to determine the presence of bromate in each bread sample. Three different bread samples were used for this analysis.

The real sample analysis of bromate in the bread samples was investigated with the constructed sensor (NIPcMWCNTs/GCE) utilizing the standard addition procedure. About 5 g of dried bread samples were ground to powder using a mortar and pestle and dissolved in distilled water to form a homogeneous paste by continuously shaking the mixture at room temperature for 60 min. The resultant paste was sufficiently diluted and left for 24 h. The solution was filtered and centrifuged at 3000 rpm to obtain a clear supernatant. The supernatant was spiked with a known bromate concentration (20, 30, and 50 μM), and the bromate content of each spiked bread sample was analyzed using the square wave voltammetry technique. The preliminary test result shows that none of the three bread samples test positive.

Table 7 summarizes the mean percentage recovery of bromate from the bread samples after a triplicate determination. The mean percentage recovery obtained for the NIPcMWCNTs/GCE sensor is 103.3%, 100.9%, and 102.8%, with the percentage relative standard deviation (% RSD) of 1.58%, 3.60%, and 2.24% for sample X, Y, and Z, respectively.

The results in Table 7 show that NIPcMWCNTs/GCE exhibited a good percentage recovery. The bromate % recovery offered by the this sensor competes favorably with similar fabricated bromate sensors in various real samples (Kirowa-Eisner et al. 1994; Zhang et al. 2022a, b). This result also established the reliability of the NIPcMWCNTs/GCE as suitable sensor for bromate detection in food products.

Table 7 Bromate analysis in bread samples at NIPcMWCNTs/GCE electrode

Bread sample	Amount added (μM)	Amount found (μM)	% Recovery	% RSD
X	20.00	20.48	102.4	1.58
	30.00	31.75	105.8	
	50.00	50.92	101.8	
Y	20.00	21.25	106.3	3.60
	30.00	29.67	98.9	
	50.00	48.72	97.4	
Z	20.00	19.88	99.4	2.24
	30.00	31.49	105.0	
	50.00	52.00	104.0	

X, Y, and Z are bread samples

Stability and reproducibility

The stability of NiPcMWCNTs/GCE was examined via CV with 20 repeated scans (75 mV s^{-1}) in 0.1 M H_2SO_4 (pH 1) with 1 mM $KBrO_3$ in it. There was only a 4.5% current drop (Fig. 13), indicating that the NiPcMWCNTs/GCE is very stable. This electrode offered high stability (95.5%) compared with other fabricated bromate sensors (Mao et al. 2015; Zhong et al. 2016).

The reproducibility of NiPcMWCNTs/GCE was investigated using cyclic voltammetry in 0.1 M H_2SO_4 (pH 1) with 1 mM $KBrO_3$ in it. The bare electrode was modified

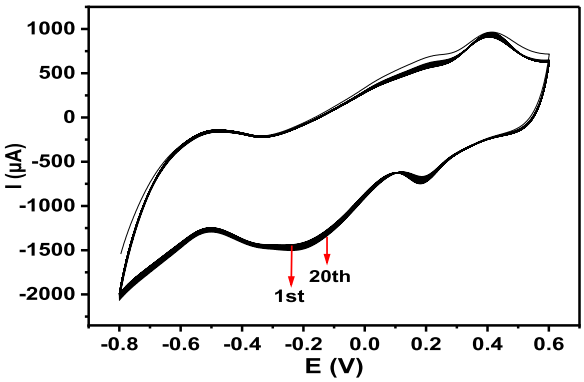

Fig. 13 Cyclic voltammograms of NiPcMWCNTs/GCE (20 scans) in 0.1 M H_2SO_4 containing 1 mM $KBrO_3$ solution (pH 1)

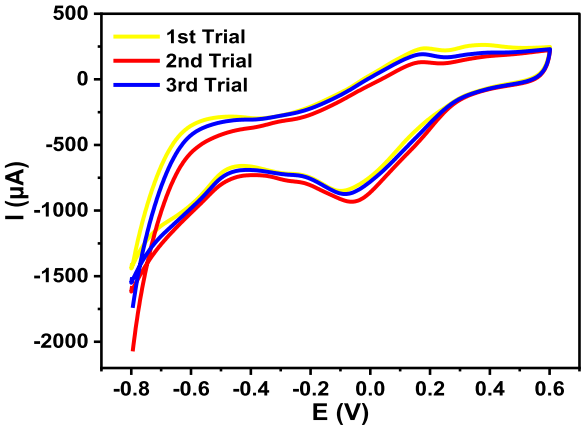

Fig. 14 Cyclic voltammograms of NiPcMWCNTs/GCE in 0.1 M H_2SO_4 containing 1 mM $KBrO_3$ solution (pH 1) at 25 mV s^{-1} (scan rate) for three different electrode modification trials

with NiPcMWCNTs nanocomposite at three different times before the electroanalysis of the bromate, and the produced cyclic voltammogram was recorded. Figure 14 depicts the NiPcMWCNTs/GCE cyclic voltammograms. After the three successive modifications, the cathodic current responses recorded for the NiPcMWCNTs/GCE gave the percentage relative standard deviation (% RSD) of 3.5%. The NiPcMWCNTs/GCE with a low % RSD, suggesting that the NiPcMWCNTs/GCE displayed a more reproducible result. The fabricated sensor offers a high reproducibility compared to various bromate sensors in literature (Li et al. 2005; Mao et al. 2014).

Conclusion

The study explored the use of the NiPcMWCNTs/GCE to detect bromate in food samples using EIS and SWV techniques. Energy dispersive X-Ray, X-ray diffraction, UV–visible spectroscopy, TEM, and SEM established the successful fabrication of the nanomaterials. The EIS and CV studies revealed that the nanocomposite modified electrode demonstrated a higher current response and a quicker electron transport capability over other modified electrodes. It also showed that the nanocomposite electrode displayed quick electron transfer capability, higher power density, and super-capacitive behaviour in the H_2SO_4 electrolyte than the other investigated electrolytes (Na_2SO_4, PBS, and SAB).

The electrochemical detection of bromate at NiPcMWCNTs/GCE via SWV gave a lower LoD and a higher sensitivity than the EIS technique. In contrast, the EIS offered a wider LDR than the SWV. The mechanism of bromate at the interface of the modified electrode surfaces of NiPcMWCNTs/GCE was found to be diffusion controlled. The developed sensor was characterized by good selectivity, high stability (95.5%), and good reproducibility (% RSD; 3.5%). The developed sensor was effectively adopted to determine bromate in bread samples with a good recovery. Thus, it is a suitable and reliable sensor for bromate detection in real samples (bread).

Acknowledgements
SAB, and OEF thank the North-West University and MaSIM for their financial support and research facilities. OEF acknowledges the FRC of North-West University and the National Research Foundation of South Africa for Thuthuka funding for Researchers (UID: 117709).

Author contributions
OEF conceptualized and designed the work and was part of the manuscript write-up. OEF, and SAB was involved in the manuscript preparation. All the authors reviewed the manuscript and agreed to publication.

Funding
Open access funding provided by North-West University. This research was funded by the National Research Foundation of South Africa for Thuthuka funding for Researchers (UID: 117709). The APC was funded by Higher Degree of North-West University, South Africa.

Availability of data and materials
The datasets used and/or analyzed during the current study are available from the corresponding author upon reasonable request.

Declarations

Competing interests
The authors declare no conflict of interest.

Received: 3 March 2023 Accepted: 10 July 2023
Published online: 20 July 2023

References

Ali B, Laffir F, Kailas L, Armstrong G, Kailas L, O'Connell R, McCormac T. Electrochemical characterisation of NiII-crown-type polyoxometalate-doped polypyrrole films for the catalytic reduction of bromate in water. Eur J Inorg Chem. 2019;2019:394–401.
Arikan K, Burhan H, Bayat R, Sen F. Glucose nano biosensor with non-enzymatic excellent sensitivity prepared with nickel–cobalt nanocomposites on f-MWCNT. Chemosphere. 2022;291:132720.
Balamurugan A, Chen SM. Silicomolybdate-doped PEDOT modified electrode: electrocatalytic reduction of bromate and oxidation of ascorbic acid. Electroanal Int J Devot Fundam Pract Asp Electroanal. 2007;19:1616–22.
Balogun SA, Fayemi OE. Effects of electrolytes on the electrochemical impedance properties of NiPcMWCNTs-modified glassy carbon electrode. Nanomaterials. 2022;12:1876.
Cao L, Chen H-Z, Li H-Y, Zhou H-B, Sun J-Z, Zhang X-B, Wang M. Fabrication of rare-earth biphthalocyanine encapsulated by carbon nanotubes using a capillary filling method. Chem Mater. 2003;15:3247–9.
Crofton K. Bromate: concern for developmental neurotoxicity? Toxicology. 2006;221:212–6.
Das G, Sain B, Kumar S. Synthesis, characterization and catalytic activity of cobalt phthalocyanine dichloride in sweetening of heavier petroleum fractions. Catal Today. 2012;198:228–32.
Ding L, Liu Y, Guo S-X, Zhai J, Bond AM, Zhang J. Phosphomolybdate@poly(diallyldimethylammonium chloride)-reduced graphene oxide modified electrode for highly efficient electrocatalytic reduction of bromate. J Electroanal Chem. 2014;727:69–77.
Eluri R, Paul B. Synthesis of nickel nanoparticles by hydrazine reduction: mechanistic study and continuous flow synthesis. J Nanopart Res. 2012;14:1–14.
Fang Y-H, Liu Z-P. Tafel kinetics of electrocatalytic reactions: from experiment to first-principles. ACS Catal. 2014;4:4364–76.
Fawell J, Walker M. Approaches to determining regulatory values for carcinogens with particular reference to bromate. Toxicology. 2006;221:149–53.
Goyal RK. Nanomaterials and nanocomposites: synthesis, properties, characterization techniques, and applications. Boca Raton: CRC Press; 2017.
Guaraldo TT, Goulart LA, Moraes FC, Lanza MR. Carbon black nanospheres modified with Cu (II)-phthalocyanine for electrochemical determination of Trimethoprim antibiotic. Appl Surf Sci. 2019;470:555–64.
Han N, Wang Y, Ma L, Wen J, Li J, Zheng H, Nie K, Wang X, Zhao F, Li Y. Supported cobalt polyphthalocyanine for high-performance electrocatalytic CO_2 reduction. Chem. 2017;3:652–64.
Haque F, Rahman M, Ahmed E, Bakshi P, Shaikh A. A cyclic voltammetric study of the redox reaction of Cu (II) in presence of ascorbic acid in different pH media. Dhaka Univ J Sci. 2013;61:161–6.
Hassan SS, Liu Y, Solangi AR, Bond AM, Zhang J. Phosphomolybdate-doped-poly (3, 4-ethylenedioxythiophene) coated gold nanoparticles: Synthesis, characterization and electrocatalytic reduction of bromate. Anal Chim Acta. 2013;803:41–6.

Hassine CBA, Kahri H, Barhoumi H. Simultaneous determination of catechol and hydroquinone using nickel nanoparticles/poly-4-nitroaniline nanocomposite modified glassy carbon electrode. IEEE Sens J. 2021;21:18864–70.
He W, Ding Y, Zhang W, Ji L, Zhang X, Yang F. A highly sensitive sensor for simultaneous determination of ascorbic acid, dopamine and uric acid based on ultra-small Ni nanoparticles. J Electroanal Chem. 2016;775:205–11.
Jiang Z, Wang Y, Zhang X, Zheng H, Wang X, Liang Y. Revealing the hidden performance of metal phthalocyanines for CO_2 reduction electrocatalysis by hybridization with carbon nanotubes. Nano Res. 2019;12:2330–4.
Kantize K, Booysen IN, Mambanda A. Electrochemical sensing of acetaminophen using nanocomposites comprised of cobalt phthalocyanines and multi-walled carbon nanotubes. J Electroanal Chem. 2019;850:113391.
Kaya EN, Tuncel S, Basova TV, Banimuslem H, Hassan A, Gürek AG, Ahsen V, Durmuş M. Effect of pyrene substitution on the formation and sensor properties of phthalocyanine-single walled carbon nanotube hybrids. Sens Actuators B Chem. 2014;199:277–83.
Kim H-J, Shin H-S. Ultra trace determination of bromate in mineral water and table salt by liquid chromatography–tandem mass spectrometry. Talanta. 2012;99:677–82.
Kirowa-Eisner E, Schwarz M, Rosenblum M, Gileadi E. Negative apparent electrochemical enthalpy of activation: the reduction of bromate at the dropping mercury electrode in alkaline solutions. J Electrochem Soc. 1994;141:1183.
Klug HP, Alexander LE. X-ray diffraction procedures: for polycrystalline and amorphous materials; 1974.
Kumar CR, Betageri VS, Nagaraju G, Pujar G, Suma B, Latha M. Photocatalytic, nitrite sensing and antibacterial studies of facile bio-synthesized nickel oxide nanoparticles. J Sci Adv Mater Devices. 2020;5:48–55.
Lee Y-G, Lee HJ, Jang A. Amperometric bromate-sensitive sensor via layer-by-layer assembling of metalloporphyrin and polyelectrolytes on carbon nanotubes modified surfaces. Sens Actuators B Chem. 2017;244:157–66.
Li Y, Bu W, Wu L, Sun C. A new amperometric sensor for the determination of bromate, iodate and hydrogen peroxide based on titania sol–gel matrix for immobilization of cobalt substituted Keggin-type cobalt-tungstate anion by vapor deposition method. Sens Actuators B Chem. 2005;107:921–8.
Li Z, Chen J, Pan D, Tao W, Nie L, Yao S. A sensitive amperometric bromate sensor based on multi-walled carbon nanotubes/phosphomolybdic acid composite film. Electrochim Acta. 2006;51:4255–61.
Li H, Xu Z, Li K, Hou X, Cao G, Zhang Q, Cao Z. Modification of multi-walled carbon nanotubes with cobalt phthalocyanine: effects of the templates on the assemblies. J Mater Chem. 2011;21:1181–6.
Li X, Li J, Wang H, Li R, Ma H, Du B, Wei Q. An electrochemiluminescence sensor for bromate assay based on a new cationic polythiophene derivative. Anal Chim Acta. 2014;852:69–73.
Li H, Pan Y, Wang Z, Yu Y, Xiong J, Du H, Lai J, Wang L, Feng S. Coordination engineering of cobalt phthalocyanine by functionalized carbon nanotube for efficient and highly stable carbon dioxide reduction at high current density. Nano Res. 2022;15:3056–64.
Luo L, Huang H, Yang Y, Gong S, Li Y, Wang Y, Luo W, Li Z. Nickel and manganese oxide heterostructure nanoparticles supported by carbon nanotube for highly efficient oxygen evolution reaction catalysis. Appl Surf Sci. 2022;575:151699.
Majidi MR, Ghaderi S, Asadpour-Zeynali K, Dastangoo H. Electrochemical determination of bromate in different types of flour and bread by a sensitive amperometric sensor based on palladium nanoparticles/graphene oxide nanosheets. Food Anal Methods. 2015;8:2011–9.
Mao R, Zhao X, Lan H, Liu H, Qu J. Efficient electrochemical reduction of bromate by a Pd/rGO/CFP electrode with low applied potentials. Appl Catal B. 2014;160:179–87.
Mao R, Zhao X, Lan H, Liu H, Qu J. Graphene-modified Pd/C cathode and Pd/GAC particles for enhanced electrocatalytic removal of bromate in a continuous three-dimensional electrochemical reactor. Water Res. 2015;77:1–12.
Mei B, Liu C, Li J, Gu S, Du X, Lu S, Song F, Xu W, Jiang Z. Operando HERFD-XANES and surface sensitive Δμ analyses identify the structural evolution of copper (II) phthalocyanine for electroreduction of CO_2. J Energy Chem. 2022;64:1–7.
Menendez-Miranda M, Fernandez-Argüelles MT, Costa-Fernandez JM, Pereiro R, Sanz-Medel A. Room temperature phosphorimetric determination of bromate in flour based on energy transfer. Talanta. 2013;116:231–6.
Mphuthi NG, Adekunle AS, Fayemi OE, Olasunkanmi LO, Ebenso EE. Phthalocyanine doped metal oxide nanoparticles on multi-walled carbon nanotubes platform for the detection of dopamine. Sci Rep. 2017;7:1–23.
Ndebele N, Sen P, Nyokong T. Electrochemical detection of dopamine using phthalocyanine-nitrogen-doped graphene quantum dot conjugates. J Electroanal Chem. 2021;886:115111.
Oliveira TM, Morais S. New generation of electrochemical sensors based on multi-walled carbon nanotubes. Appl Sci. 2018;8:1925.
Puangjan A, Chaiyasith S, Taweeporngitgul W, Keawtep J. Application of functionalized multi-walled carbon nanotubes supporting cuprous oxide and silver oxide composite catalyst on copper substrate for simultaneous detection of vitamin B2, vitamin B6 and ascorbic acid. Mater Sci Eng C. 2017;76:383–97.
Qiu S, Li Y, Xu H, Liang Q, Zhou M, Rong J, Li Z, Xu S. Efficient catalytic oxidation of benzyl alcohol by tetrasubstituted cobalt phthalocyanine-MWCNTs composites. Solid State Sci. 2022;129:106905.
Rahali Y, Benmoussa A, Ansar M, Benziane H, Lamsaouri J, Idrissi M, Draoui M, Zahidi A, Taoufik J. A simple and rapid method for spectrophotometric determination of bromate in bread. Electr J Environ Agric Food Chem. 2011;10:5245.
Reddy KV. Sensitive and reliable electrochemical detection of nitrite and H2O2 embellish-CoPc coupled with appliance of composite MWCNTs. Anal Chim Acta. 2020;1108:98–107.
Roodbari NJ, Omrani A, Hosseini SR. Synthesis, characterization and performance of a novel Ni–Co/GO-TiO_2 for electrooxidation of methanol and ethanol. Int J Hydrogen Energy. 2022;47:6044–58.
Shanmugavel V, Santhi KK, Kurup AH, Kalakandan S, Anandharaj A, Rawson A. Potassium bromate: effects on bread components, health, environment and method of analysis: a review. Food Chem. 2020;311:125964.
Shao W, Mai J, Wei Z. Nonenzymatic lactic acid detection using cobalt polyphthalocyanine/carboxylated multi-walled carbon nanotube nanocomposites modified sensor. Chemosensors. 2022;10:83.
Shi E, Zou X, Liu J, Lin H, Zhang F, Shi S, Liu F, Zhu G, Qu F. Electrochemical fabrication of copper-containing metal–organic framework films as amperometric detectors for bromate determination. Dalton Trans. 2016;45:7728–36.
Snyder SA, Vanderford BJ, Rexing DJ. Trace analysis of bromate, chlorate, iodate, and perchlorate in natural and bottled waters. Environ Sci Technol. 2005;39:4586–93.
Vilian AE, Chen S-M, Kwak CH, Hwang S-K, Huh YS, Han Y-K. Immobilization of hemoglobin on functionalized multi-walled carbon nanotubes-poly-l-histidine-zinc oxide nanocomposites toward the detection of bromate and H_2O_2. Sens Actuators B Chem. 2016;224:607–17.
Wang L, Pan D, Zhou M, Liang Q, Li Z. Effect of phthalocyanines supported carbon nanotube for the catalytic oxidation of benzyl alcohol. Solid State Sci. 2021;113:106546.
Wierzbicka E, Sulka GD. Nanoporous spongelike Au–Ag films for electrochemical epinephrine sensing. J Electroanal Chem. 2016;762:43–50.
Winiarski JP, de Barros MR, Wecker GS, Nagurniak GR, Parreira RLT, Affeldt RF, Peralta RA, Jost CL. A novel hybrid organic–inorganic silsesquioxane and cobalt (ii) tetrasulphophthalocyanine material as an efficient electrochemical sensor for the simultaneous determination of the anti-hypertensive nifedipine and its metabolite. J Mater Chem C. 2020;8:6839–50.
World Health Organization (WHO). Guidelines for drinking-water quality: world health organization. 2004.
Wu ZG, Munoz M, Montero O. The synthesis of nickel nanoparticles by hydrazine reduction. Adv Powder Technol. 2010;21:165–8.
Wu X, Xing W, Zhang L, Zhuo S, Zhou J, Wang G, Qiao S. Nickel nanoparticles prepared by hydrazine hydrate reduction and their application in supercapacitor. Powder Technol. 2012;224:162–7.
Yadav KK, Ahmad S, Narang U, Bhattacharya S, Chauhan S. Xanthenedione substituted metallophthalocyanines as an efficient and recyclable catalyst for one–pot three component synthesis of 3-substituted indoles. ChemistrySelect. 2016;1:3635–9.

Zakaria P, Bloomfield C, Shellie RA, Haddad PR, Dicinoski GW. Determination of bromate in sea water using multi-dimensional matrix-elimination ion chromatography. J Chromatogr A. 2011;1218:9080–5.
Zangeneh Kamali K, Alagarsamy P, Huang NM, Ong BH, Lim HN. Hematite nanoparticles-modified electrode based electrochemical sensing platform for dopamine. Sci World J. 2014;2014:457.
Zhang Y, Zhang Y, Li L, Chen J, Li P, Huang W. One-step in situ growth of high-density POMOFs films on carbon cloth for the electrochemical detection of bromate. J Electroanal Chem. 2020;861:113939.
Zhang S, Cheng H, Wang B, Shi F, Yan L, Zeng L, Li L, He S, Sun W. An electrochemical biosensor based on hemoglobin and FeS@ MoS2-C nanocomposite for nitrite, hydrogen peroxide and bromate detection. Int J Electrochem Sci. 2022a;17:2.
Zhang W, Xiahou C, Ji X, Zhang Y, Zhang H, Song S, Niu X. Utilization of molybdenum disulfide-graphene aerogel composite for hemoglobin-based electrochemical sensor for highly sensitive detection of bromate. Int J Electrochem Sci. 2022b;17:2.
Zhong Y, Yang Q, Li X, Yao F, Xie L, Zhao J, Chen F, Xie T, Zeng G. Electrochemically induced pitting corrosion of Ti anode: Application to the indirect reduction of bromate. Chem Eng J. 2016;289:114–22.
Zhou D-D, Ding L, Cui H, An H, Zhai J-P, Li Q. Fabrication of high dispersion Pd/MWNTs nanocomposite and its electrocatalytic performance for bromate determination. Chem Eng J. 2012;200:32–8.

Publisher's Note